

An Integrated Attribute Guided Dense Attention Model for Fine-Grained Generalized Zero-Shot Learning

Tasfia Shermin^{a,*}, Shyh Wei Teng^a, Ferdous Sohel^b, Manzur Murshed^a,
Guojun Lu^a

^a*School of Engineering, Information Technology and Physical Sciences, Federation
University, Churchill-3842, Australia*

^b*Discipline of Information Technology, Mathematics and Statistics, Murdoch University,
WA-6150, Australia*

Abstract

Embedding learning (EL) and feature synthesizing (FS) are two of the popular categories of fine-grained GZSL methods. The global feature exploring EL or FS methods do not explore fine distinction as they ignore local details. And, the local detail exploring EL or FS methods either neglect direct attribute guidance or global information. Consequently, neither method performs well. In this paper, we propose to explore global and direct attribute-supervised local visual features for both EL and FS categories in an integrated manner for fine-grained GZSL. The proposed integrated network has an EL sub-network and a FS sub-network. Consequently, the proposed integrated network can be tested in two ways. We propose a novel two-step dense attention mechanism to discover attribute-guided local visual features. We introduce new mutual learning between the sub-networks to exploit mutually beneficial information for optimization. Moreover, to reduce bias towards the source domain during testing, we propose to compute source-target class similarity based on mutual information and transfer-learn the target classes. We demonstrate that our proposed method outperforms contemporary methods on benchmark datasets.

Keywords: Generalized zero-shot learning, fine-grained classification, dense attention mechanism

1. Introduction

Conventional supervised deep learning classifiers require a large amount of labeled training data and the test instances to be from the training categories to achieve a satisfactory performance. Although ordinary object images are easily accessible, there are many object categories with scarce visual data, such

*Corresponding author

Email address: t.shermin@federation.edu.au (Tasfia Shermin)

as endangered categories of plants and animals [1, 2, 3]. To address the issues, *Zero-shot learning* (ZSL) methods are studied. ZSL methods aim to exploit the visual-semantic relationship of source (seen) classes to extend the traditional classification task to target (unseen) classes that have no available training images. ZSL methods have two main categories: inductive (no target images used during training) [4, 5, 6] and transductive (unlabelled target images used in training) [7, 8, 9]. This work focuses on the inductive setting. Inductive ZSL methods aim to train a visual classifier on source classes and test the classifier on target classes only. The underlying distribution of source and target domains is disjoint. The ZSL setting assumes that the trained visual classifier knows whether a test sample belongs to the source or target classes. To reduce the restriction of this unrealistic assumption, the ZSL setting is extended to a more advanced and realistic setting called Generalized Zero-Shot Learning (GZSL) [9, 10, 11, 12], where the classifier has to classify test images from both source and target classes.

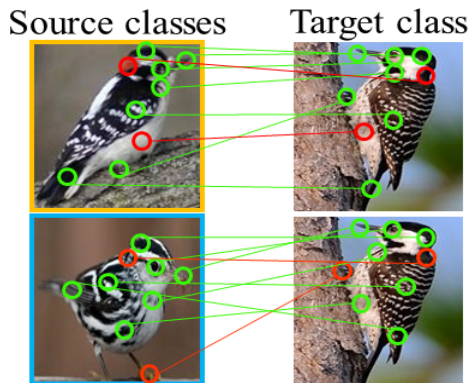


Figure 1: Samples from CUB dataset showing only a few dissimilar attributes between the source and target classes. Red and green indicators denote dissimilar and similar attributes, respectively. Best viewed in color.

The ultimate aim of this work is to improve GZSL for fine-grained recognition. Unlike the coarse-grained datasets (classes, e.g., Animal, Table, and Bus, with no sub-ordinate classes), the classification of fine-grained datasets (with sub-ordinate classes, e.g., different types of birds(Blue jay, Florida jay, and Green jay)) demands more local discriminative properties. The region-based local features capture more fine distinctive information and relevance to the semantic attributes than the global features (Figure 1).

Embedding learning (non-generative) and feature synthesizing (generative) methods are two popular categories of approaches for GZSL methods. Most existing embedding learning GZSL methods learn an embedding function for aligning or mapping the global visual features of a source class image with its class semantic vector for GZSL tasks [5, 6, 13, 14, 15, 16]. The feature synthesizing GZSL methods also learn to generate high-level or global image features using Generative Adversarial Networks (GAN) conditioned on the class

semantic vectors [17, 12, 18, 19, 20, 21] for GZSL tasks.

Some embedding learning works [22, 23, 15, 24] have used the region-based local informative features. However, they explore indirect guidance from semantic descriptors; they do not relate individual attributes to the local features; rather, they relate a combination of all attributes. Consequently, they do not fully explore the discriminative local visual-semantic information, which is important for fine-grained GZSL recognition. Existing fine-grained embedding learning GZSL methods [22, 23, 15, 24, 25] ignore global visual information. Since the final goal of GZSL methods is to learn visual classifiers, ignoring global details will harm the generic structure of the deep neural network’s visual representation. Therefore, besides exploring local details for improved fine-grained GZSL, we want to preserve global details for constructing a better visual GZSL classifier.

We aim to address the aforementioned limitations in both embedding learning and feature synthesizing methods. As such, we propose an integrated network, which has an embedding learning sub-network (Attribute Guided Attention Network (AGAN)) and a feature synthesizing sub-network (Adversarial Feature Generation Network (AFGN)). First, we divide an image sample into local regions. Then, we preserve the global representation of the local regions. After that, for discovering fine-discriminative information, we explore the relation between the semantic attributes and the local region features by using our proposed two-step dense attention mechanism. Next, both the sub-networks leverage the constructed feature embedding, which comprises of our explored global and local information. Finally, both sub-networks leverage the proposed mutual learning-based optimization to assist each other in learning to construct better features for the GZSL task.

The proposed two-step dense attention mechanism uses direct attribute supervision to construct a visual feature embedding that holds *attribute-weighted local visual* information required for fine-grained classification. In particular, to assign the first-level of attention to the region features, we explore two general questions i.e., ‘Is the region related to any attribute?’ and ‘Which attribute has the most relevance to the region?’. Thus, a region’s attention has information about the presence of attributes and the most relevant attribute in the region. This will encourage only the most relevant attribute to a region to be attended and assist in learning fine distinction. In the second-level, we infuse the confidence score of having that attribute in the class so that the attention of a region containing an attribute that has a greater class score is higher weighted than others. This knowledge will encourage a better focus on common intra-class information, thereby facilitating improved class decisions. The dense-attention mechanism is placed in AGAN. We design the connection between AGAN and AFGN in such a way that they both can leverage the attribute-weighted features constructed by the attention mechanism.

We explore source-target class similarity, based on shared information, to learn target classes in AGAN loosely to reduce bias towards source classes. Mutual learning explores mutually useful information between AGAN and AFGN. Thus, the source class bias in AFGN is also partially smoothed out. Moreover, AFGN is flexible as it can be replaced with any sophisticated feature synthesiz-

ing network to learn attribute guided local features.

The testing sequence of the embedding learning GZSL methods is simple. Once the model is trained, these methods use both test images, and semantic descriptors of target classes [25, 23, 26, 24] to classify or recognize the target domain images. On the contrary, the feature synthesizing GZSL methods [12, 27, 19, 20] use the semantic descriptors of the target classes to generate visual features using the source trained model. Then, train a supervised visual classifier with the generated features. Then the trained visual classifier is used for classifying the test images of target classes. Since the proposed integrated network has both embedding learning (AGAN) and feature synthesizing sub-network (AFGN), the proposed method can test in two ways, following the test sequence of both embedding learning and feature synthesizing GZSL methods. Thus, the proposed integrated network will contribute to the GZSL field in two different fine-grained classification methods.

The main contributions of this paper are as follows:

- We propose to integrate an embedding learning sub-network and a feature generation sub-network to an integrated network. We introduce mutual learning to optimize both sub-networks. This is the first work to apply mutual learning in this domain to the best of our knowledge. The integration also enables two different ways of testing capability.
- We propose a novel two-step attention mechanism, which discovers fine distinctive local visual information directly supervised by the attributes. In addition, unlike existing fine-grained GZSL methods, we propose to preserve global visual information for developing a better GZSL visual classifier.
- For fine-grained GZSL tasks, we introduce the exploration of attribute guided fine-distinctive visual features in both embedding learning and feature synthesizing networks in a unified way.
- To reduce the bias towards source classes during testing [2, 25], we propose to transfer-learn a target class from the most similar source class based on the *pointwise mutual information* (pmi) score.
- We present an extensive empirical evaluation on several fine-grained datasets to demonstrate the superior state-of-the-art performance of the proposed method compared to contemporary GZSL and ZSL methods.

Section 2 presents a brief discussion about contemporary methods. The proposed method is described in Section 3. Results and analysis of the proposed method on various datasets are provided in Section 4.

2. Related Work

In this section, we provide a brief overview of existing embedding learning and feature synthesizing ZSL and GZSL methods.

2.1. Embedding Learning Methods

The embedding learning methods map either visual features to the semantic space [28, 29] or semantics to the visual space [30, 31] based on seen classes for the GZSL task. Most of the existing embedding learning ZSL methods use global visual features to classify fine-grained datasets. This may inject noise and non-discriminative information in the embedding [3, 6, 5].

To explore local fine-grained details, a few works have applied attention mechanisms. However, some of them do not explore proper guidance from attributes [22, 23, 15, 24] and others ignore local visual details [13, 14, 32].

A recent attention-based work [25] for fine-grained GZSL limits the feature exploration space to the number of attributes to construct attribute embedding and requires expensive attribute selection. As our ultimate goal is to learn a visual classifier, unlike [25], we construct a visual feature embedding, which retains necessary global visual features and the feature regions linked to the attributes are assigned more attention than other regions.

A non-fine-grained attention-based GZSL method, APN [33], integrates the exploration of both global and local details for GZSL tasks. The global module in APN is separated from the local module and the global module extracts channel-wise global information. This may create incompatibility in the network. On the other hand, we preserve local region-wise global information. Consequently, for building the feature embedding, we can maintain better synchronization of global features with the attribute-weighted local region features. The local module in APN aims to construct attributes from the local visual regions for GZSL, which is different than our local feature exploration (discussed in Section 3.1.1).

Moreover, in contrary to recent attention-based methods [25, 33], we propose to employ two-level of dense attention mechanism to capture and highlight finer details for fine-grained tasks.

2.2. Feature Synthesizing Methods

Feature synthesizing methods adversarially learn to synthesize visual features from class semantics and reduce the GZSL to a standard supervised classification task [19, 27, 28, 17, 21, 18, 34]. For generation of unseen class features, f-clsgGAN [19], CVAE [18], SE-GZSL [17] used conditional Generative Adversarial Networks (GANs) or Variational Autoencoders (VAE).

The feature synthesizing methods learn to generate global visual features conditioned on the attribute descriptions and ignore local distinctive details [12, 27, 19, 20, 18, 21]. On the other hand, in this paper, we explore local information related to the attributes for synthesizing features in the proposed AFGN network for improved fine-grained zero-shot recognition.

2.3. Reducing Bias Towards Source Domain

To overcome bias towards source domain, ZSL methods have explored novelty detection and prediction calibration [25, 35]. For transfer learning target classes, [9] relies on the reconstruction of source class semantic vectors from

3.1. Proposed GZSL

The proposed method addresses the limitation of existing embedding learning and feature synthesizing methods that ignore individual attributes for guiding feature embedding construction. The method shown in Figure 2 comprises two networks: 1) Attribute Guided Attention Network (AGAN) and 2) Adversarial Feature Generation Network (AFGN). AGAN is the embedding learning part of the proposed method. The attention mechanism is placed in AGAN. First, AGAN constructs feature embedding using the attention mechanism and leverages the feature embedding for the GZSL task. Then, the feature synthesizing part, AFGN, uses the constructed feature embedding to learn the generation of attribute-weighted visual features adversarially. Furthermore, AGAN and AFGN are mutually optimized to improve each other’s performance i.e., AGAN takes supervision from AFGN for optimizing the constructed feature embedding, and AFGN takes supervision from AGAN to generate visual features. This optimization is performed by minimizing our designed losses.

3.1.1. Attribute Guided Attention Network

First, we select local visual regions and preserve region-wise global information. Then we statistically bound the local regions to filter out irrelevant information. Then, the two-step dense attention mechanism constructs an attribute-weighted features. In Figure 2, the blue and green shaded parts on AGAN show the two levels of attention mechanism, respectively. Then AGAN constructs the feature embedding utilizing the output of the attention mechanism. The feature embedding holds global representation, redundancy-free, and attribute-weighted local visual information (the probability of the most relevant attribute to the visual regions and the likelihood of having that attribute in the class). Finally, a classifier utilizes the feature embedding to infer class decisions. To reduce the source class bias while learning the classifier, we optimize a transfer learning loss.

Constructing Visual Regions. For simplicity and consistency, in line with [37] and [25], we divide an image I into r equal sized regions, I_1, \dots, I_r . We use a CNN to extract features for the r regions. For example, the feature vector of the i^{th} region is $f_i = f_{\Theta}(I_i)$, where Θ denotes parameters of the CNN. Note that the CNN is frozen.

Exploring Global Information. To learn global discriminative features compatible with the local region features, we apply region-wise global average pooling on the local feature vectors $F = \{f_i\}_{i=1}^r$. This operation provides us with a feature vector $F_g \in \mathbb{R}^r$, where F_{g_i} represents the average global information of the i^{th} local region feature f_i .

Learning Relevant Information. To reduce highly irrelevant information from the extracted local feature space $F = \{f_i\}_{i=1}^r$, we bound the information propagation from F to F' . This will reduce the interruption of redundant information in the attribute-weighted feature embedding. Mutual information (MI) is used to bound M network to stop propagating irrelevant information to F' .

We employ a variational upper bound of MI [38] as,

$$I(F'; F) \leq \mathbb{E}_{p(f)} [D_{KL} [p_M(f'|f) \| r(f')]], \quad (1)$$

where $p_M(f'|f)$ is the conditional probability of the region features f' , which holds only important information depending on the extracted real region-features f . D_{KL} and $r(f')$ denote the Kullback-Leibler divergence and variational approximation of the marginal probability distribution, respectively. Note that we do not reduce feature regions or filter out redundancy from global features [12], which may lose important visual information and harm the image's visual feature representation. We remove redundancy from the feature regions to use only the relevant information within a region.

First-level Dense Attention. Now, we aim to construct a dense connection i.e, every attribute is to be connected to every visual region to explore the relevance between every attribute and every visual region. Therefore, we form a matrix F'' . The rows of F'' represent the bounded features of each region. The corresponding attribute semantic vectors \mathbf{v} are converted to V' matrix by using Q network, where the A^{th} row represents the $\mathbf{v}'_A{}^{th}$ attribute. Both M and Q are neural networks with non-linear activation function ReLU.

F'' and V' are fused as $J = F'' \otimes V'$, where \otimes denotes matrix multiplication, $F'' \in \mathbb{R}^{r \times m}$, r is the number of regions and m is the dimension of region features f' . Similarly, $V' \in \mathbb{R}^{n \times A}$, A denotes the number of attributes and n denotes the dimension of attribute vectors \mathbf{v}' , where $m = n$ is ensured by M and Q networks. The matrix multiplication ensures a dense connection between F'' and V' as the product contains information of every attribute (columns) in every regional feature (rows). The output of the matrix multiplication is $J \in \mathbb{R}^{r \times A}$ and we denote the i^{th} region as J_i , where $J_i \in \mathbb{R}^A$.

Existing attention-based GZSL works [23, 25, 26], have adopted soft attention [39] to only predict . On the other hand, we propose to use soft attention to predict the most relevant attribute to every region besides predicting the presence of attributes in the regions. A conceptual view of assigning attention to a region is shown in Figure 3.

The K network takes J matrix and applies a soft-attention normalization to set different degrees of attention to the r regions. The attentions indicate the confidence of the presence of attributes in a region. We learn individual soft-attentions for every one of the r regions using $\{T_i\}_{i=1}^r$ neural networks, which encourages to learn to attend only the most relevant attribute to a region. This definitive attention assignment facilitates the embedding to hold fine distinctive information. The attention assignment in K and $\{T_i\}_{i=1}^r$ networks are performed as follows,

$$\begin{aligned} PI &= \text{softmax}(\tanh(J^\top W_B)W_A), \\ t_i &= \text{softmax}(\tanh(J_i W_{TA_i})W_{TB_i}), \alpha_i = \lambda_\alpha PI_i H_{t_i}, \end{aligned} \quad (2)$$

where K is a neural network with learned parameters W_A and W_B and output $PI \in \mathbb{R}^r$. W_{TA_i} and W_{TB_i} are learned parameters of T_i^{th} network. The softmax

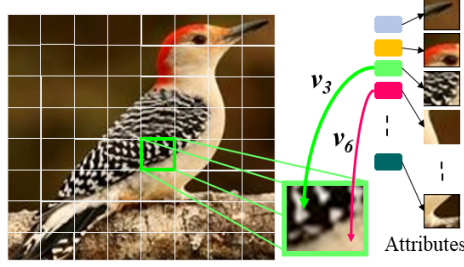


Figure 3: A conceptual illustration of the first-level attention mechanism of the proposed attribute-weighted visual feature embedding. Note that if a region has more than one attributes, then the attention of the attribute having highest confidence is assigned to the region, e.g., attribute v_3 ('wing pattern stripped') wins over v_6 ('belly color white'). Thus, presence of attribute and the most relevant attribute to a region is attended.

outputs of T_i is $t_i \in \mathbb{R}^A$, which can be treated as soft attentions of the attributes on the i^{th} feature region. The attribute yielding the highest softmax probability is most likely to have greater relevance to the i^{th} feature region than others. Thus, we consider only the highest softmax probability H_{t_i} . It also helps the attention module to focus and learn only one attribute per visual region for better discriminative learning. Similarly, we compute the soft attentions for each of the r regions using $\{T_i\}_{i=1}^r$. α_i denotes the attention and the parameter λ_α helps to avoid negligible attention. Note, to handle $\{T_i\}_{i=1}^r$ networks simultaneously, we use depth-wise (grouped) convolution; please see Section 3.1.3 for more details.

We obtain the weighted feature regions by applying the inferred soft attention as $\widehat{F''}_i = \alpha_i F''_i$. To preserve both noise-free and semantic guided visual information, we combine the attribute-weighted region features with the redundancy-free region features as follows,

$$\tilde{F}_{1_i} = F''_i \oplus \widehat{F''}_i, \quad (3)$$

where, \oplus denotes region-wise summation.

Second-level Dense Attention. To further infuse the probability of the presence of an attribute in the class in \tilde{F}_{1_i} and boost the weighted feature regions for handling more sophisticated cases, we apply another level of attention mechanism. This assists the attention mechanism in learning to assign a higher weight to a region that may contain an attribute which is more likely to be present in the class samples and helps in making a better class decision.

First, we construct the visual-semantic matrix as $\tilde{J} = \tilde{F}_1 \otimes V'$, which has the similar dimensional properties as J matrix. Then, we combine the class semantic vector a as $J' = \tilde{J}a$, where a vector is multiplied to each row of \tilde{J} matrix element-wise and $J' \in \mathbb{R}^{r \times A}$. The second-level soft attention $\tilde{\alpha}$ is computed by using J' matrix and \tilde{K} network similar to the first part (PI) of (2) i.e., $\tilde{\alpha} = \text{softmax}(\tanh(J'^T W'_B) W'_A)$, where W'_B and W'_A are learned parameters of \tilde{K} network. The feature embedding $\tilde{F}_2 \in \mathbb{R}^{r \times m}$ is constructed by summation of \tilde{F}_1 and $\tilde{F}'_1 = \tilde{\alpha} \tilde{F}_1$ as (3).

Feature Embedding. To hold the global information in the feature embedding, we apply a region-wise product between \tilde{F}_2 and F_g , i.e., the feature vector F_g is element-wise multiplied to all the column vectors of \tilde{F}_2 matrix and the dimension of \tilde{F}_2 is preserved as is. This operation infuses the region-based global information to \tilde{F}_2 . To retain all the extracted information in the final embedding, we apply an average pooling over the m -dimension of \tilde{F}_2 . Then, we concatenate the pooled features and form the final feature embedding fs , where $fs \in \mathbb{R}^m$.

AGAN-GZSL Task. Finally, f_s is fed into the classifier h_2 , which is a neural network with one hidden fully-connected layer and a softmax layer. The classifier takes f_s as input and produces $|C^s + C^t|$ -dimensional output, where the first $|C^s|$ indices represent the source classes and the remaining indices represent the target classes. The class scores are computed as $p(s_i) = \exp(s_i) / \sum_{c \in |C^s|} \exp(s_i^c)$, where $s = h_2(f_s)$, $h_2(f_s) \in \mathbb{R}^{|C^s + C^t|}$, $|C^s + C^t|$ is the total number of source and target classes.

3.1.2. Adversarial Feature Generation Network

In this section, we present the proposed AFGN, which utilizes final feature embedding f_s from AGAN to learn to generate features that are highly related to the attributes for fine-grained classification.

The AFGN can adopt any adversarial feature synthesizing GZSL method. In this work, we adopt a feature generation method f-WGAN [19], which has a visual feature generator G and a discriminator D . The f-WGAN takes random Gaussian noise ϵ and the class semantic vector a as inputs and learns to generate a visual feature $\tilde{x} \in \mathcal{X}$ of class y . The idea is to train G to generate features of the source class images x^s conditioned on a_c^s so that during testing, the generator G can repurpose its learned knowledge to generate target class features only from a_c^t . In f-WGAN [19], the global features (i.e., x^s) are used as the real features to guide G . On the contrary, we propose to utilize our attribute-weighted features for the guidance. Not only our features are associated with attribute attention, they also hold redundancy-free information. For converting the semantic vectors to visual features, the usage of f_s inferred from AGAN will assist the AFGN to follow the underlying dependency between the semantic and visual feature spaces. Therefore, we optimize,

$$\mathcal{L}_{WGAN} = E[D(f_s, a)] - E[D(\tilde{x}, a)] - \lambda E \left[(\|\nabla_{\hat{x}} D(\hat{x}, a)\|_2 - 1)^2 \right], \quad (4)$$

where $\tilde{x} = G(\epsilon, a)$, λ denotes the penalty coefficient, and $\hat{x} = \eta f_s + (1 - \eta)\tilde{x}$ with $\eta \sim U(0, 1)$. To further ensure the learned features hold discriminative properties suitable for classification and less bias towards source classes, we use the h_2 from AGAN as follows,

$$\mathcal{L}_{cls} = -E_{\tilde{x} \sim p_{\tilde{x}}(\tilde{x})} [\log P(y | \tilde{x}; \theta)], \quad (5)$$

where y is the true class label of \tilde{x} and $P(y | \tilde{x}; \theta)$ denotes the probability of \tilde{x} being predicted as y by h_2 .

3.1.3. Grouped Convolution Attention Block

We replace $\{T_i\}_{i=1}^r$ fully-connected neural networks with grouped 1D convolutional block. Everyone of the r T_i networks has two linear layers, one is followed by *tanh* function and the other has a *softmax* function after it. We replace the linear layers, as shown in Figure 4. We use a kernel size of 1 in the convolutional block to mimic the linear or fully-connected neural layers. The input of the convolution block has $b \times (A * r) \times 1$ -dimension, where b , A , r , and $*$ denote the batch size, number of attributes, number of regions, and multiplication respectively. In Figure 4, h denotes the size of the hidden layer of T_i . Note that in the first conv layer, r_i^{th} group will be connected to only A input channels and in the second conv layer r_i^{th} group will be connected to h input channels (hidden layer neurons). Thus, the weights of different groups in the convolution block are not shared, which supports our goal to learn separate attentions for r regions parallelly. After the second conv layer we obtain an output of $b \times (A * r) \times 1$ -dimension which is reshaped to $b \times r \times A$ -dimension for applying softmax over the A attributes of r regions.

```
nn.conv1d(in_channels = A * r, out_channels = h * r,
kernel_size = 1, groups = r)

nn.Tanh()

nn.conv1d(in_channels = h * r, out_channels = A * r,
kernel_size = 1, groups = r)
```

Figure 4: Grouped convolution pseudo-code.

3.2. Optimization

In this section, we present the loss optimization details of the proposed method.

3.2.1. Mutual Learning

Since both AGAN and AFGN use the attribute-weighted feature embedding f_s to learn their tasks, we utilize both networks to assist one-another through mutual learning. We define the mutual learning losses for AGAN and AFGN networks as follows,

$$\mathcal{L}_{m1} = \frac{1}{2} \|f_s - \tilde{x}\|_2^2, \mathcal{L}_{m2} = \frac{1}{2} \|\tilde{x} - f_s\|_2^2, \quad (6)$$

where, $\tilde{x} = G(\epsilon, a)$. By optimizing \mathcal{L}_{m1} , AGAN utilizes the reconstruction power of G in AFGN to facilitate its embedding learning. On the other hand, AFGN uses the learned embedding in AGAN to improve its reconstruction ability by optimizing \mathcal{L}_{m2} .

3.2.2. Loss Optimization in AGAN

For the source classes, we optimize the standard cross-entropy loss as,

$$\mathcal{L}_{ce} = \frac{1}{ns} \sum_{i=1}^{ns} \mathcal{L}(h_2(f_{s_i}), y_i), \quad (7)$$

where y_i is the true class label of f_{s_i} and ns denotes the number of samples.

To smooth out bias towards source classes, we hope to loosely learn a target class from the knowledge of its closest source class. Thus, we propose to optimize the following loss over the target class indices in h_2 in one-vs-rest fashion,

$$\mathcal{L}_u = \sum_{i=1}^{ns} \sum_{N=C^s+1}^{C^s+C^t} pmi_{ij} \log P(y = j|f_{s_i}) - (1 - pmi_{ij}) \log(1 - P(y = j|f_{s_i})). \quad (8)$$

Here, pmi_{ij} is the similarity measure between the class of i^{th} source sample and j^{th} target class and $P(y = j|f_{s_i})$ means the probability of j^{th} index given the feature of its closest source class.

To measure class similarity, we adopt pointwise mutual information (pmi). In information theory, pmi measures association and co-occurrence between two events of two discrete random variables. In the fine-grained GZSL setup, the target classes share many attributes with the source classes. Therefore, the random variables of the class semantic vectors of source classes a_c^s will pose significant statistical dependence with that of target classes a_c^t . This implies that the target classes will produce higher pmi for similar source classes in the class semantic vector space. We convert a_c of the source and target classes to probability distributions by applying a softmax function.

Let, $Z_{\mathcal{A}^s}$ and $Z_{\mathcal{A}^t}$ represent the converted probability distributions of the source and target classes. The pmi between two individual events $Z_{\mathcal{A}^s}^i$ and $Z_{\mathcal{A}^t}^j$ of the two discrete random variables $Z_{\mathcal{A}^s}$ and $Z_{\mathcal{A}^t}$ can be computed as,

$$pmi(Z_{\mathcal{A}^s}^i; Z_{\mathcal{A}^t}^j) = \log \frac{P(Z_{\mathcal{A}^s}^i, Z_{\mathcal{A}^t}^j)}{P(Z_{\mathcal{A}^s}^i)P(Z_{\mathcal{A}^t}^j)}. \quad (9)$$

We construct the joint probability distribution as $Jn = Z_{\mathcal{A}^t} \cdot Z_{\mathcal{A}^s}^\top$ (tensor Jn has a dimension of $C^t \times C^s$), and $Z_{\mathcal{A}^t}$ and $Z_{\mathcal{A}^s}$ matrices hold the dimension of $C^t \times a_c^t$ and $C^s \times a_c^s$. The marginals are computed from the summation of rows and columns of Jn . The final objective for the AGAN network becomes,

$$\begin{aligned} & \mathcal{L}_{ce} + \lambda_p \mathcal{L}_u + \lambda_{m1} \mathcal{L}_{m1} \\ \text{s.t. } & \mathbb{E}_{p(f)} [D_{KL} [p_{Mi}(f' | f) \| r(f')]] \leq \gamma, \end{aligned} \quad (10)$$

where λ_p and λ_{m1} are a hyper-parameters to weight the losses for target classes and mutual learning respectively, and γ is the MI bound.

3.2.3. Loss Optimization in AFGN

The final objective of AFGN is as follows,

$$\min_G \max_D \mathcal{L}_{WGAN} + \lambda_{cls} \mathcal{L}_{cls} + \lambda_{m2} \mathcal{L}_{m2}. \quad (11)$$

Here, λ_{cls} and λ_{m2} are hyper-parameters for weighting the contribution of \mathcal{L}_{cls} in the optimization and mutual learning respectively. We train AGAN and AFGN in an end-to-end fashion. During each iteration, first, we sample a mini-batch from $(x_i^s, y_i^s)_{i=1}^{n_s}$ and Gaussian noise ϵ . Then we update the learnable components of AGAN by (10). Finally, we update the learnable components of AFGN by (11).

3.3. Testing Phase.

Once the AGAN is trained, we formulate the classification score of a test instance as $P_{GZSL}(x_i) = \max_i \{s_i\}_{i=1}^{C^t}$ and $P_{ZSL}(x_i) = \max_i \{s_i\}_{i=C^s+1}^{C^t}$. For AFGN, we use the trained generator G and re-sampled ϵ to generate multiple synthetic features for every source and target class. Then, we learn a separate supervised classifier, which produces $|C^s + C^t|$ and $|C^t|$ dimensional outputs for GZSL and ZSL. We define the classification loss as $\mathcal{L}_{h_{AFGN}} = -E_{x' \sim p'} [\log P(y | x'; \theta_{h_{AFGN}})]$, where x' , y , and p' denote samples of the newly formed training dataset, the true class label of x' , and distribution of the new training dataset respectively. $P(y | x'; \theta_{h_{AFGN}})$ represents the probability of x' being recognized as y .

4. Experimental Studies

In this section, we describe the datasets, evaluation protocol, implementation details, experimental outcomes, hyper-parameter settings, ablative analysis, and learned attention visualization.

4.1. Datasets

In line with fine-grained GZSL method [25], we conduct our experiments on three popular fine-grained datasets, Caltech-UCSD Birds-200-2011 (CUB) [40], SUN Attribute (SUN) [41], and Animals with Attributes 2 (AWA2) [42]. We further extend our experiments to Animals with Attributes 1 (AWA1) [4] dataset, which is a version of AWA2 dataset. We follow [2], to split the total classes into source and target classes on each dataset.

CUB contains a total of 11,788 images of 200 classes of fine-grained bird species, among them, 150 are selected as source classes, and the remaining 50 classes are treated as the target or unseen classes. **SUN** is composed of 14,340 images with 717 categories of scenes. This dataset is widely used for fine-grained scene recognition and GZSL. The number of source and target classes used for GZSL are 645 and 72, respectively. **AWA1** consists of 30,475 images of 50 different sub-ordinate classes of animals. For GZSL, 40 classes are used as source, and 10 are used as target classes. **AWA2** has 40 source and 10 target classes comprising 37,322 images in total.

4.2. Evaluation Metrics:

We evaluate the performance of our method by per-class Top-1 accuracy. For the source domain, we will evaluate the Top-1 accuracy on source classes denoted as S . For the target domain, the Top-1 accuracy on the target classes is represented as T . For evaluating the total performance of GZSL, we compute the harmonic mean in line with [2] as, $H = (2 \times S \times T)/(S + T)$.

4.3. Implementation Details.

In our experiments, we extract a feature map of size $7 \times 7 \times 2048$ from the last convolutional block of pre-trained ResNet-101 and use it as a set of features from 7×7 local regions. It is worth mentioning that the pre-trained ResNet-101 model is only used for feature extraction and not fine-tuned in the training procedure. In AGAN, the networks M , Q , and h_2 are fully-connected neural networks with no hidden layers. The networks K and \tilde{K} have only one hidden layer. The threshold γ for MI bound in the region features is cross-validated between $[0.01, 0.05]$. The attribute semantic vectors \mathbf{v} for all datasets are extracted from Wikipedia articles trained GloVe model [36]. The attention balancing hyper-parameter λ_α is set to 10. Since the generator has to produce fully-connected features from conditional input, we maintain a full fully-connected structure of the generator for efficiency i.e., the generator has only one hidden fully-connected layer. The discriminator has no hidden layers in the structure. Adam solver with $\beta_1 = 0.5$, $\beta_2 = 0.999$ and learning rate 0.0001 is used for optimization. The suitable hyper-parameters setting across all datasets is as follows, $\lambda_p \in [0.1, 0.2, 0.3, 0.4]$, $\lambda_{m1} = 0.1$, $\lambda_{cls} = 0.1$, and $\lambda_{m2} = 0.2$.

Approach	Model	GZSL											
		CUB			SUN			AWA1			AWA2		
		T	S	H	T	S	H	T	S	H	T	S	H
\triangle	LATEM [6] (2016)	15.2	57.3	24.0	-	-	-	7.3	71.7	13.3	11.5	77.3	20.0
	DEM [1] (2017)	19.6	57.9	29.2	-	-	-	32.8	84.7	47.3	30.5	86.4	45.1
	DCN [35] (2018)	28.4	60.7	38.7	25.5	37.0	30.2	25.5	84.2	39.1	-	-	-
	AREN [15] (2019)	38.9	78.7	52.1	19.0	38.8	25.5	-	-	-	15.6	92.9	26.7
	CRnet [16] (2019)	45.5	56.8	50.5	34.1	36.5	35.3	58.1	74.7	65.4	-	-	-
	TCN [9] (2019)	52.6	52.0	52.3	31.2	37.3	34.0	49.4	76.5	60.0	61.2	65.8	63.4
	DVBE [10] (2020)	53.2	60.2	56.5	45.0	37.2	40.7	-	-	-	63.6	70.8	67.0
	DAZLE [25] (2020)	56.7	59.6	58.1	52.3	24.3	33.2	-	-	-	60.3	75.7	67.1
	VSG-CNN [11] (2020)	52.6	62.1	57.0	30.3	31.6	30.9	-	-	-	60.4	75.1	67.0
	APN [33] (2020)	65.3	69.3	67.2	41.9	34.0	37.6	-	-	-	56.5	78.0	65.5
	AGAN (Ours)	67.9	71.5	69.7	40.9	42.9	41.8	65.1	83.2	73.0	64.1	80.3	71.3
\square	SE-GZSL [17] (2018)	41.5	53.3	46.7	40.9	30.5	34.9	56.3	67.8	61.5	58.3	68.1	62.8
	f-CLSWGAN [19] (2018)	43.7	57.7	49.7	42.6	36.6	39.4	57.9	61.4	59.6	-	-	-
	f-VAEGAN-D2 [21] (2019)	48.4	60.1	53.6	45.1	38.0	41.3	-	-	-	57.6	70.6	63.5
	LisGAN [20] (2019)	46.5	57.9	51.6	42.9	37.8	40.2	52.6	76.3	62.3	-	-	-
	GMN [27] (2019)	56.1	54.3	55.2	53.2	33.0	40.7	61.1	71.3	65.8	-	-	-
	RFF-GZSL (softmax) [12] (2020)	52.6	56.6	54.6	45.7	38.6	41.9	59.8	75.1	66.5	-	-	-
	TF-VAEGAN [43] (2020)	52.8	64.7	58.1	45.6	40.7	43.0	59.8	75.1	66.6	-	-	-
	ASPN [34] (2020)	50.7	61.5	55.6	-	-	-	58.0	85.7	69.2	46.2	87.0	60.4
	E-PGN [44] (2020)	52.0	61.1	56.2	-	-	-	62.1	83.4	71.2	52.6	83.5	64.6
	APN [33] + f-VAEGAN-D2 [21] (2020)	65.7	74.9	70.0	49.4	39.2	43.7	-	-	-	62.2	69.5	65.6
	AFGN (Ours)	69.8	77.1	73.2	53.1	45.9	49.2	67.5	83.8	74.7	68.1	82.9	74.7

Table 1: Performance comparison. T and S are the Top-1 accuracies tested on target classes and source classes, respectively, in GZSL. H is the harmonic mean of T and S.

4.4. Results and Analysis

In this section, we analyze the evaluation of the proposed and contemporary GZSL methods. The ZSL results of LATEM [6], DEM [1], and SGMAL [24] are adopted from SGMAL [24], GZSL results of LATEM [6] and DEM [1] are taken from ASPN [34], and the results of other compared methods are obtained from their corresponding published articles. For a fair comparison, we compare both AGAN and AFGN with only inductive methods and synthesize 400 features per class for comparing AFGN’s performance. In Tables 1 and 2, \triangle and \square denote embedding learning and feature synthesizing methods, respectively, and ‘-’ represents that the results are not reported.

4.4.1. Generalized Zero-Shot Learning.

Table 1 shows that both AGAN and AFGN achieves more Harmonic mean H (9) compared to contemporary methods. H the main indicator of how well a GZSL method performs. AGAN and AFGN also significantly outperform the contemporary methods for the majority of the GZSL tasks. Unlike embedding learning methods, feature synthesizing methods leverage supervised training on synthesized data during testing and outperform embedding learning methods. Similarly, AFGN outperforms AGAN. AGAN outperforms all the compared embedding learning methods, which either use local or global feature embedding. This indicates that the proposed method’s feature embedding holds finer discriminative information required for fine-grained tasks. The improved performance of AGAN also proves that both global and local information plays a vital role in fine-grained GZSL.

APN [33] is the closest competitor, which has a global feature learning module (BaseMod) along-with a local feature learning module (ProtoMod). AGAN outperforms APN significantly. AFGN increases the accuracy of GZSL by a large margin compared to APN + f-VAEGAN-D2 [21]. This means the proposed method is more effective for GZSL tasks. Considering fine-grained attention-based GZSL methods, DAZLE [25] is the closest competitor, which leverages only local region-based features. However, DAZLE restricts the embedding space to the number of selective attributes. In comparison, we preserve all local region features highlighted by the most relevant attributes to the regions and the global information corresponding to the local regions. The improved performance of AGAN and AFGN verifies the effectiveness of our feature embedding.

Concerning irrelevant information removing GZSL methods, RFF-GZSL [12] filters out redundant information from global features. On the other hand, the proposed method preserves global information on average to hold the generic trend of deep classifier features and removes redundancy from local regions to reduce the interruption of irrelevant information. The higher performance of AGAN and AFGN validates that the proposed feature embedding holds better distinctive and necessary information. Compared to other methods, AGAN reduces the source domain bias by optimizing the target loss \mathcal{L}_u and makes better knowledge transfer from source to target classes. AFGN follows the same trend as it uses the discriminative knowledge of h_2 .

4.4.2. Zero-Shot Learning

The performance of ZSL tasks (CUB, SUN, AWA1) of different methods is shown in Table 2. As expected, the results show that the target class accuracy of all ZSL methods is higher than the GZSL tasks. The proposed AGAN and AFGN perform better than contemporary methods. The improved performance of the networks for ZSL tasks shows that the trained networks gain the ability to generalize well to unseen target classes even in the conventional ZSL setup, which is encouraged by the optimization of \mathcal{L}_u based on the pmi similarity.

Approach	Model	CUB	SUN	AWA1	Approach	Model	CUB	SUN	AWA1
Δ	LATEM [6]	49.4	-	78.4	\square	SE-GZSL [17]	60.3	64.5	83.8
	DEM [1]	51.8	-	80.3		cycle-CLSWGAN [18]	58.6	59.9	66.8
	S ² GA (2-attention layer) [23]	68.9	-	-		LisGAN [20]	58.8	61.7	70.6
	S ² GA (3-attention layer) [23]	68.5	-	-		GMN [27]	64.3	63.6	71.9
	SGMAL [24]	70.5	-	83.5		f-CLSWGAN [19]	57.3	60.8	68.2
	TCN [9]	59.5	61.5	70.3		SABR [45]	65.2	62.8	-
	DAZLE [25]	67.8	-	-		f-VAEGAN [21]	72.9	65.6	-
	AGAN (Our)	74.9	66.5	88.7		AFGN (our)	78.5	69.8	89.1

Table 2: Performance comparison of ZSL tasks.

4.4.3. Hyper-parameters Analysis.

For studying the trend of GZSL accuracy of AGAN and AFGN in different hyper-parameters (λ_P , λ_{m1} , λ_{m2} , and λ_{cls}) settings, we plot the graphs shown in Figure 5.

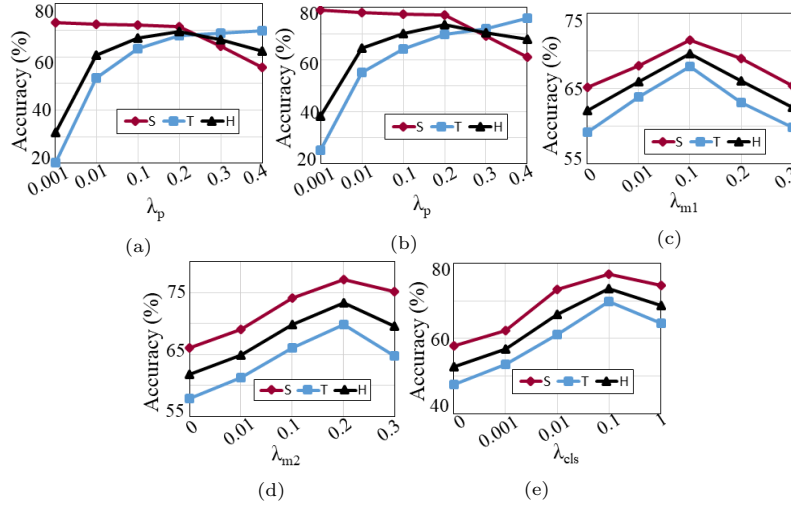


Figure 5: Effect of varying the hyper-parameters in the GZSL performance on the CUB dataset.

Figures 5(a) and 5(b) show the performance of AGAN and AFGN with various λ_P setups respectively. In case of both the networks, we observe that the source accuracy depicts a sharp decreasing pattern after $\lambda_P = 0.2$ while

the target accuracy starts to surpass the source accuracy a little after that point. This means the networks gradually lose the capability to recognize the source domain samples correctly. The harmonic mean H achieves the optimal performance at $\lambda_P = 0.2$ and decreases soon after that. Thus, we find the value of $\lambda_P = 0.2$ optimal for the task. Note that for other datasets we cross-validate λ_P in the range $[0.001, 0.01, 0.1, 0.2, 0.3, 0.4]$.

The effect of different settings of the hyper-parameters weighting the mutual loss λ_{m1} in AGAN and λ_{m2} in AFGN are shown in Figures 5(d) and 5(e) respectively. We observe that the optimal performance in AGAN is achieved when $\lambda_{m1} = 0.1$, and the source and target classes performances are harmed when the value of λ_{m1} is greater than that. On the other hand, the AFGN network has low accuracies for fewer values of λ_{m2} and achieves optimal performance when λ_{m2} is 0.2. This means the AFGN is more facilitated by mutual learning compared to AGAN.

Figure 5(c) illustrates the performance of AFGN in different settings of λ_{cls} . Note that AFGN has a very low source and target accuracy for near-zero values of λ_{cls} , which indicates the importance of the discriminative feedback of h_2 in the network. We demonstrate that the performance increases for greater values of λ_{cls} , however, decreases slightly after $\lambda_{cls} = 0.1$. Therefore, we set the value of λ_{cls} to 0.1 for optimal performance in AFGN.

4.4.4. MI Bound Analysis

Figure 6 shows the change in performances of AGAN and AFGN on different values of γ . Both networks show low accuracy near zero MI bound, which indicates interruption of redundant information in the features.

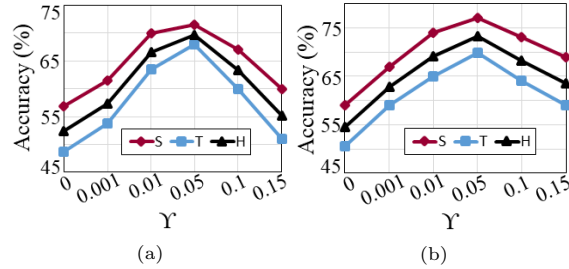


Figure 6: Performance comparison for different MI bounds γ of AGAN (a) and AFGN (b) on GZSL task of the CUB dataset.

Note that the performance of both networks depicts an increasing trend with the increasing values of γ . However, after $\gamma = 0.05$, the performance starts to decrease, which means the necessary information flow is harmed. Both the networks achieve optimal performance when the MI bound is $\gamma = 0.05$. Note that for some datasets we observe better performance at $\gamma = 0.01$, therefore we mentioned earlier $\gamma \in [0.01, 0.05]$.

4.4.5. Ablation Study

To justify the role of different components in AGAN and AFGN separately, we present the ablative analysis in Table 3. We perform the ablative analysis by deducting different vital components from AGAN and AFGN and show their impact on the performances.

Approach	T	S	H	Approach	T	S	H
AGAN w/o γ	48.7	56.8	52.4	AFGN w/o γ	50.5	59.1	54.4
AGAN (f_s w/o \mathcal{L}_u)	20.1	72.5	31.4	AFGN (f_s w/o \mathcal{L}_u)	25.2	78.9	38.1
AGAN (f_s w/ \tilde{F}_1)	58.1	61.9	51.2	AFGN (f_s w/ \tilde{F}_1)	60.9	70.1	56.6
-	-	-	-	AFGN w/o \mathcal{L}_{cls}	47.8	58.1	52.4
AGAN w/o \mathcal{L}_{m1}	59.2	65.2	62.0	AFGN w/o \mathcal{L}_{m2}	57.9	66.1	61.7
AGAN w/o F_g	59.9	65.3	62.4	AFGN w/o F_g	62.4	68.7	65.3
AGAN w/o m	61.2	66.9	63.9	AFGN w/o m	62.5	72.8	67.2
AGAN	67.9	71.5	69.7	AFGN	69.8	77.1	73.2

Table 3: Ablative analysis for GZSL on the CUB dataset.

First, we study the importance of MI bound γ on the proposed method by exploring the variants AGAN w/o γ and AFGN w/o γ . The accuracy of AGAN decreases drastically without the MI bound. AFGN without the MI bound shows a little better performance than AGAN. The existence of irrelevant information in the local regions while constructing the feature embedding harms AGAN and AFGN for fine-grained GZSL recognition. Thus, the MI bound is crucial for the proposed method.

We refer to the variants f_s w/o \mathcal{L}_u as feature embedding without the target loss. We observe that both AGAN and AFGN variants show high S accuracy and very low T accuracy. This indicates that without \mathcal{L}_u , AGAN and AFGN struggle to generalize to target classes, which demonstrates the importance of the target loss based on pmi similarity.

The variants of AGAN and AFGN where the feature embedding is formed with only a one-step dense attention mechanism (f_s w/ \tilde{F}_1) show a tremendous decrease in performance. This justifies that only one-level of dense attention mechanism is not sufficient enough to yield satisfactory performance.

In AFGN w/o \mathcal{L}_{cls} , the performance decreases drastically as the discriminative property of the generated features are not monitored during training.

To analyze the impact of mutual training in AGAN and AFGN, we explore the variants AGAN w/o \mathcal{L}_{m1} and AFGN w/o \mathcal{L}_{m2} . For these two variants, AGAN and AFGN are trained jointly. However, in one variant, AGAN does not optimize \mathcal{L}_{m1} and in the other AFGN does not optimize \mathcal{L}_{m2} . The results indicate that AFGN is more facilitated than AGAN by mutual learning.

For analyzing the influence of global features in the proposed method, we exploit the two variants AGAN w/o F_g and AFGN w/o F_g . We observe that the performance of both networks decreases to a great extent. This verifies the impact of the global features besides local features in the performance of GZSL tasks.

To study the impact of mutual learning in the proposed method, we implement both AGAN and AFGN without training them jointly i.e., first, we

train AGAN separately and then use the feature embedding from AGAN to train AFGN. These two variants are denoted by AGAN w/o m and AFGN w/o m . The degrading performance of the two variants shows the impact of the interaction between AGAN and AFGN during optimization.

4.4.6. Analyzing Number of Generated Features

For analyzing the effect of the number of generated features per class during testing, we plot the graphs in Figures 7(a), 7(b) and 7(c).

The graphs (Figures 7(a) and 7(b)) show the performance comparison of CUB and SUN datasets with respect to a various number of generated features per class for GZSL. In general, we demonstrate that with the increasing number of features per class, the H increases. For CUB dataset, S and T significantly

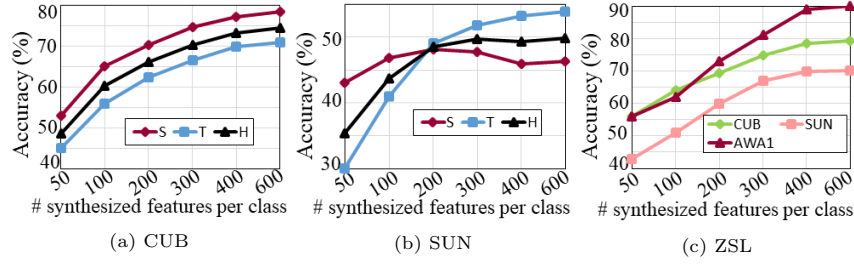


Figure 7: (a) and (b) Increasing the number of synthesized features wrt GZSL performance in CUB and SUN datasets. (c) Increasing the number of synthesized features wrt ZSL performance in CUB, SUN, and AWA1 datasets.

increase till 400, and after that the increment is marginal. For SUN dataset, S marginally decreases after 200; however, T increases with the increasing number of features per class. Notice that after 400, the value of H plateaus as both S and T depict no significant change. We demonstrate that AFGN can generalize well to unseen target classes besides seen source classes.

For ZSL (Figure 7(c)), the performance of all the datasets significantly increases with the increasing number of synthesized features per class. More number of features per class helps the final classifier learn better and generalize more to unseen target classes. Similar to GZSL tasks, we observe that the increment in performance is marginal after 400. The improved generalization to target classes in GZSL and ZSL tasks validates that AFGN reduces source domain bias.

4.4.7. Analyzing Two-level of Attentions

The first row of Figure 8 presents some examples of the class ‘Mallard’ from the CUB dataset.

To study the learned attention, we visualize the learned attention maps for an image of the class ‘Mallard’ in the second row of Figure 8. We visualize the output of the first level of attention in the second column of the second row, which shows that the local regions linked to the attributes are assigned

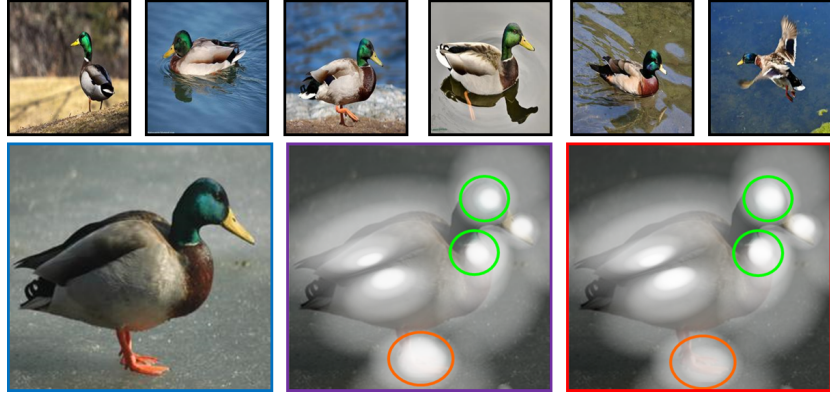


Figure 8: Samples from ‘Mallard’ class of CUB dataset (first row). Visualization of the learned attention maps (second row), where first, second, and third columns show the original images, images after applying one-step attention (α), and two-step attention (α and $\tilde{\alpha}$), respectively. Best viewed in color.

more weights than the other regions. This assists in focusing better on the possible distinctive attributed regions. The third column of the second row shows the visualization of second-level attention. Compared to the output of one-level attention, two-level attention shows more weight assignment on the regions having intra-class common attributes to assist in better class decisions. In particular, notice that the region shown in **green** circles in the third column achieve more attention compared to that of the second column as the attributes ‘forehead color green’ and ‘breast color grey’ have a greater score of presence in the samples of the class. On the other hand, the region shown in **orange** circle in the third column receives less attention than the second column as the attribute ‘leg color orange’ has less visibility in the samples of the class. This visualization verifies the importance of our two-step attention mechanism to learn better attribute-weighted features for fine-grained GZSL.

5. Conclusion

This paper proposes an integrated GZSL method with an embedding learning sub-network (AGAN) and a feature synthesizing sub-network (AFGN). This unification avails two-way testing capability. The sub-networks learn to solve the GZSL task by utilizing global features and the attribute-weighted local visual features constructed based on the proposed two-step dense attention mechanism. We explore mutual information between the semantic descriptors of the source and target classes to learn target classes based on source-target class similarity and reduce source domain bias. The proposed method also exploits mutually beneficial information between the two sub-networks through mutual-training. We show that both the learned GZSL networks outperform contemporary methods on various datasets.

References

- [1] H. Zheng, J. Fu, T. Mei, J. Luo, Learning multi-attention convolutional neural network for fine-grained image recognition, in: Proceedings of the IEEE International Conference on Computer Vision, 2017, pp. 5209–5217.
- [2] Y. Xian, B. Schiele, Z. Akata, Zero-shot learning-the good, the bad and the ugly, in: Proceedings of the IEEE Conference on Computer Vision and Pattern Recognition, 2017, pp. 4582–4591.
- [3] Y. Zhu, M. Elhoseiny, B. Liu, X. Peng, A. Elgammal, A generative adversarial approach for zero-shot learning from noisy texts, in: Proceedings of the IEEE Conference on Computer Vision and Pattern Recognition, 2018, pp. 1004–1013.
- [4] C. H. Lampert, H. Nickisch, S. Harmeling, Learning to detect unseen object classes by between-class attribute transfer, in: Proceedings of the IEEE Conference on Computer Vision and Pattern Recognition, 2009, pp. 951–958.
- [5] Z. Zhang, V. Saligrama, Zero-shot learning via joint latent similarity embedding, in: Proceedings of the IEEE Conference on Computer Vision and Pattern Recognition, 2016, pp. 6034–6042.
- [6] Y. Xian, Z. Akata, G. Sharma, Q. Nguyen, M. Hein, B. Schiele, Latent embeddings for zero-shot classification, in: Proceedings of the IEEE Conference on Computer Vision and Pattern Recognition, 2016, pp. 69–77.
- [7] Y. Fu, T. M. Hospedales, T. Xiang, S. Gong, Transductive multi-view zero-shot learning, *IEEE transactions on pattern analysis and machine intelligence* 37 (11) (2015) 2332–2345.
- [8] Y. Yu, Z. Ji, X. Li, J. Guo, Z. Zhang, H. Ling, F. Wu, Transductive zero-shot learning with a self-training dictionary approach, *IEEE transactions on cybernetics* 48 (10) (2018) 2908–2919.
- [9] H. Jiang, R. Wang, S. Shan, X. Chen, Transferable contrastive network for generalized zero-shot learning, in: Proceedings of the IEEE/CVF International Conference on Computer Vision, 2019, pp. 9765–9774.
- [10] S. Min, H. Yao, H. Xie, C. Wang, Z.-J. Zha, Y. Zhang, Domain-aware visual bias eliminating for generalized zero-shot learning, in: Proceedings of the IEEE/CVF Conference on Computer Vision and Pattern Recognition, 2020, pp. 12664–12673.
- [11] C. Geng, L. Tao, S. Chen, Guided cnn for generalized zero-shot and open-set recognition using visual and semantic prototypes, *Pattern Recognition* 102 (2020) 107263.

- [12] Z. Han, Z. Fu, J. Yang, Learning the redundancy-free features for generalized zero-shot object recognition, in: Proceedings of the IEEE/CVF Conference on Computer Vision and Pattern Recognition, 2020, pp. 12865–12874.
- [13] Y. Guo, G. Ding, J. Han, S. Tang, Zero-shot learning with attribute selection, in: Proceedings of the AAAI Conference on Artificial Intelligence, Vol. 32, 2018.
- [14] Y. Liu, J. Guo, D. Cai, X. He, Attribute attention for semantic disambiguation in zero-shot learning, in: Proceedings of the IEEE/CVF International Conference on Computer Vision, 2019, pp. 6698–6707.
- [15] G.-S. Xie, L. Liu, X. Jin, F. Zhu, Z. Zhang, J. Qin, Y. Yao, L. Shao, Attentive region embedding network for zero-shot learning, in: Proceedings of the IEEE Conference on Computer Vision and Pattern Recognition, 2019, pp. 9384–9393.
- [16] F. Zhang, G. Shi, Co-representation network for generalized zero-shot learning, in: International Conference on Machine Learning, 2019, pp. 7434–7443.
- [17] V. Kumar Verma, G. Arora, A. Mishra, P. Rai, Generalized zero-shot learning via synthesized examples, in: Proceedings of the IEEE Conference on Computer Vision and Pattern Recognition, 2018, pp. 4281–4289.
- [18] R. Felix, I. Reid, G. Carneiro, et al., Multi-modal cycle-consistent generalized zero-shot learning, in: Proceedings of the European Conference on Computer Vision, 2018, pp. 21–37.
- [19] Y. Xian, T. Lorenz, B. Schiele, Z. Akata, Feature generating networks for zero-shot learning, in: Proceedings of the IEEE Conference on Computer Vision and Pattern Recognition, 2018, pp. 5542–5551.
- [20] J. Li, M. Jing, K. Lu, Z. Ding, L. Zhu, Z. Huang, Leveraging the invariant side of generative zero-shot learning, in: Proceedings of the IEEE Conference on Computer Vision and Pattern Recognition, 2019, pp. 7402–7411.
- [21] Y. Xian, S. Sharma, B. Schiele, Z. Akata, f-vaegan-d2: A feature generating framework for any-shot learning, in: Proceedings of the IEEE Conference on Computer Vision and Pattern Recognition, 2019, pp. 10275–10284.
- [22] Z. Akata, M. Malinowski, M. Fritz, B. Schiele, Multi-cue zero-shot learning with strong supervision, in: Proceedings of the IEEE Conference on Computer Vision and Pattern Recognition, 2016, pp. 59–68.
- [23] Z. Ji, Y. Fu, J. Guo, Y. Pang, Z. M. Zhang, et al., Stacked semantics-guided attention model for fine-grained zero-shot learning, in: Advances in Neural Information Processing Systems, 2018, pp. 5995–6004.

- [24] Y. Zhu, J. Xie, Z. Tang, X. Peng, A. Elgammal, Semantic-guided multi-attention localization for zero-shot learning, in: *Advances in Neural Information Processing Systems*, 2019.
- [25] D. Huynh, E. Elhamifar, Fine-grained generalized zero-shot learning via dense attribute-based attention, in: *Proceedings of the Conference on Computer Vision and Pattern Recognition*, 2020, pp. 4483–4493.
- [26] D. Huynh, E. Elhamifar, A shared multi-attention framework for multi-label zero-shot learning, in: *Proceedings of the Conference on Computer Vision and Pattern Recognition*, 2020, pp. 8776–8786.
- [27] M. B. Sariyildiz, R. G. Cinbis, Gradient matching generative networks for zero-shot learning, in: *Proceedings of the IEEE Conference on Computer Vision and Pattern Recognition*, 2019, pp. 2168–2178.
- [28] H. Huang, C. Wang, P. S. Yu, C.-D. Wang, Generative dual adversarial network for generalized zero-shot learning, in: *Proceedings of the IEEE conference on computer vision and pattern recognition*, 2019, pp. 801–810.
- [29] E. Kodirov, T. Xiang, S. Gong, Semantic autoencoder for zero-shot learning, in: *Proceedings of the IEEE Conference on Computer Vision and Pattern Recognition*, 2017, pp. 3174–3183.
- [30] Y. Shigeto, I. Suzuki, K. Hara, M. Shimbo, Y. Matsumoto, Ridge regression, hubness, and zero-shot learning, in: *Joint European Conference on Machine Learning and Knowledge Discovery in Databases*, 2015, pp. 135–151.
- [31] L. Zhang, T. Xiang, S. Gong, Learning a deep embedding model for zero-shot learning, in: *Proceedings of the IEEE Conference on Computer Vision and Pattern Recognition*, 2017, pp. 2021–2030.
- [32] L. Huang, W. Wang, J. Chen, X.-Y. Wei, Attention on attention for image captioning, in: *Proceedings of the IEEE International Conference on Computer Vision*, 2019, pp. 4634–4643.
- [33] W. Xu, Y. Xian, J. Wang, B. Schiele, Z. Akata, Attribute prototype network for zero-shot learning, in: *Advances of the Neural Information Processing Systems*, 2020.
- [34] Z. Lu, Y. Yu, Z.-M. Lu, F.-L. Shen, Z. Zhang, Attentive semantic preservation network for zero-shot learning, in: *Proceedings of the IEEE Conference on Computer Vision and Pattern Recognition Workshops*, 2020, pp. 682–683.
- [35] S. Liu, M. Long, J. Wang, M. I. Jordan, Generalized zero-shot learning with deep calibration network, in: *Advances in Neural Information Processing Systems*, 2018, pp. 2005–2015.

- [36] J. Pennington, R. Socher, C. D. Manning, Glove: Global vectors for word representation, in: *Proceedings of the Conference on Empirical Methods in Natural Language Processing (EMNLP)*, 2014, pp. 1532–1543.
- [37] K. Xu, J. Ba, R. Kiros, K. Cho, A. Courville, R. Salakhudinov, R. Zemel, Y. Bengio, Show, attend and tell: Neural image caption generation with visual attention, in: *International conference on machine learning*, 2015, pp. 2048–2057.
- [38] A. A. Alemi, I. Fischer, J. V. Dillon, K. Murphy, Deep variational information bottleneck, in: *Proceedings of the International Conference on Learning Representations*, 2017.
- [39] D. Bahdanau, K. Cho, Y. Bengio, Neural machine translation by jointly learning to align and translate, in: *Proceedings of the International Conference on Learning Representations*, 2015.
- [40] P. Welinder, S. Branson, T. Mita, C. Wah, F. Schroff, S. Belongie, P. Perona, Caltech-ucsd birds 200, California Institute of Technology.
- [41] G. Patterson, J. Hays, Sun attribute database: Discovering, annotating, and recognizing scene attributes, in: *Proceedings of the IEEE Conference on Computer Vision and Pattern Recognition*, 2012, pp. 2751–2758.
- [42] Y. Xian, C. H. Lampert, B. Schiele, Z. Akata, Zero-shot learning—a comprehensive evaluation of the good, the bad and the ugly, *IEEE transactions on pattern analysis and machine intelligence* 41 (9) (2018) 2251–2265.
- [43] S. Narayan, A. Gupta, F. S. Khan, C. G. Snoek, L. Shao, Latent embedding feedback and discriminative features for zero-shot classification, in: *Proceedings of the European Conference on Computer Vision*, 2020.
- [44] Y. Yu, Z. Ji, J. Han, Z. Zhang, Episode-based prototype generating network for zero-shot learning, in: *Proceedings of the IEEE Conference on Computer Vision and Pattern Recognition*, 2020, pp. 14035–14044.
- [45] A. Paul, N. C. Krishnan, P. Munjal, Semantically aligned bias reducing zero shot learning, in: *Proceedings of the IEEE Conference on Computer Vision and Pattern Recognition*, 2019, pp. 7056–7065.